

## Mapping the Influence of Molecular Structure on Rates of Electron Transfer Using Direct Measurements of the Electron Spin–Spin Exchange Interaction

Aaron S. Lukas, Patrick J. Bushard, Emily A. Weiss, and Michael R. Wasielewski\*

*Contribution from the Department of Chemistry & Center for Nanofabrication and Molecular Self-Assembly, Northwestern University, Evanston, Illinois 60208-3113*

Received October 23, 2002; E-mail: wasielew@chem.northwestern.edu

**Abstract:** The spin–spin exchange interaction,  $2J$ , in a radical ion pair produced by a photoinduced electron transfer reaction can provide a direct measure of the electronic coupling matrix element,  $V$ , for the subsequent charge recombination reaction. We have developed a series of dyad and triad donor–acceptor molecules in which  $2J$  is measured directly as a function of incremental changes in their structures. In the dyads the chromophoric electron donors 4-(*N*-pyrrolidiny)- and 4-(*N*-piperidiny)naphthalene-1,8-dicarboximide, 5ANI and 6ANI, respectively, and a naphthalene-1,8:4,5-bis(dicarboximide) (NI) acceptor are linked to the *meta* positions of a phenyl spacer to yield 5ANI–Ph–NI and 6ANI–Ph–NI. In the triads the same structure is used, except that the piperidine in 6ANI is replaced by a piperazine in which a *para*-*X*-phenyl, where *X* = H, F, Cl, MeO, and Me<sub>2</sub>N, is attached to the *N'* nitrogen to form a *para*-*X*-aniline (XAn) donor to give XAn–6ANI–Ph–NI. Photoexcitation yields the respective 5ANI<sup>+</sup>–Ph–NI<sup>–</sup>, 6ANI<sup>+</sup>–Ph–NI<sup>–</sup>, and XAn<sup>+</sup>–6ANI–Ph–NI<sup>–</sup> singlet radical ion pair states, which undergo subsequent radical pair intersystem crossing followed by charge recombination to yield <sup>3</sup>NI. The radical ion pair distances within the dyads are about 11–12 Å, whereas those in the triads are about ~16–19 Å. The degree of delocalization of charge (and spin) density onto the aniline, and therefore the average distance between the radical ion pairs, is modulated by the *para* substituent. The <sup>3</sup>NI yields monitored spectroscopically exhibit resonances as a function of magnetic field, which directly yield  $2J$  for the radical ion pairs. A plot of  $\ln 2J$  versus  $r_{DA}$ , the distance between the centroids of the spin distributions of the two radicals that comprise the pair, yields a slope of  $-0.5 \pm 0.1$ . Since both  $2J$  and  $k_{CR}$ , the rate of radical ion pair recombination, are directly proportional to  $V^2$ , the observed distance dependence of  $2J$  shows directly that the recombination rates in these molecules obey an exponential distance dependence with  $\beta = 0.5 \pm 0.1 \text{ \AA}^{-1}$ . This technique is very sensitive to small changes in the electronic interaction between the two radicals and can be used to probe subtle structural differences between radical ion pairs produced from photoinduced electron transfer reactions.

### Introduction

The spin dynamics of photogenerated radical ion pairs are sensitive to external applied magnetic fields, which permit the manipulation of both the radical ion pair lifetimes and the yields of products arising from radical ion pair decay.<sup>1–3</sup> However, the presence of a large isotropic spin–spin exchange interaction,  $2J$ , between singlet and triplet radical ion pair states often inhibits the mixing of these states that is necessary for the observation of magnetic field effects (MFEs) at easily accessible magnetic fields. For this reason MFEs are most often observed in radical ion pairs that are either freely diffusing<sup>4</sup> or tethered via long polymethylene linkers to ensure that  $2J$  is small.<sup>5</sup> In these systems efficient charge separation (CS) occurs in an

encounter complex, which is followed by diffusive separation of the radical ions or conformational changes in the linked systems, both of which increase the distance between the radical ions, allowing  $2J$  to diminish. Such flexibility results in a wide distribution of radical ion pair conformations and distances, thereby complicating analysis of how the magnitude of  $2J$  correlates with the specific structure of the radical ion pair and the distance between the two radical ions. Staerk and co-workers have shown that D–A compounds both with fully flexible polymethylene linkers and with polymethylene linkers incorporating a *trans*-cyclohexyl group to limit their conformational freedom sometimes exhibit a resonance in the magnetic field dependence of the triplet yield following radical ion pair recombination.<sup>5,6</sup>

The bacterial photosynthetic reaction center is the classic example of a rigid system that displays large MFEs on the yield of its triplet charge recombination product. Electron transport within photosynthetic bacteria is initiated by electron transfer

- (1) Steiner, U. E.; Ulrich, T. *Chem. Rev.* **1989**, *89*, 51–147.
- (2) Grissom, C. B. *Chem. Rev.* **1995**, *95*, 3–24.
- (3) Hoff, A. J.; Gast, P.; van der Vos, R.; Franken, E. M.; Lous, E. J. Z. *Phys. Chem.* **1993**, *180*, 175–192.
- (4) Schulten, K.; Staerk, H.; Weller, A.; Werner, H.-J.; Nickel, B. Z. *Phys. Chem.* **1976**, *101*, 371–390.
- (5) Staerk, H.; Kuhnle, W.; Treichel, R.; Weller, A. *Chem. Phys. Lett.* **1985**, *188*, 19–24.

- (6) Werner, U.; Kuhnle, W.; Staerk, H. *J. Phys. Chem.* **1993**, *97*, 9280–9287.

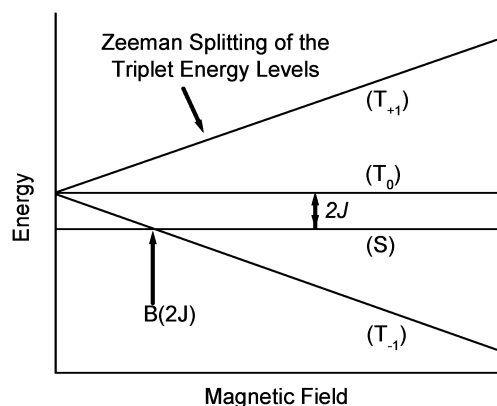


**Figure 1.** Radical ion pair energy levels as a function of magnetic field.

from the lowest excited state of a bacteriochlorophyll dimer (P) to an adjacent bacteriochlorophyll (B), followed by sequential thermal electron transfers to bacteriopheophytin (H), and finally to a quinone (Q),<sup>7–11</sup> forming the  $P^+B-H-Q^-$  radical ion pair in about 200 ps. Removal or chemical reduction of Q, followed by photoexcitation produces the  $P^+B-H^-$  radical ion pair, which is formed in a pure singlet state. The  $^1[P^+B-H^-]$  radical ion pair singlet state undergoes radical pair intersystem crossing (RP-ISC) by mixing with the three sublevels of the triplet state,  $^1[P^+B-H^-] \leftrightarrow ^3[P^+B-H^-]$ , driven primarily by the electron–nuclear hyperfine interactions in each radical ion of the pair. Subsequent radical ion pair recombination (CR) produces  $^3P-B-H$ . Application of a magnetic field as small as 0.01 T lowers the yield of  $^3P-B-H$  by about 40%,<sup>12</sup> which is attributed to Zeeman splitting of the triplet sublevels that diminishes mixing between the singlet and two of the three triplet radical ion pair states, Figure 1.

Despite many studies of rigid D–A arrays synthesized to mimic the electron transfer dynamics of photosynthetic bacteria, spin selective CR to a localized triplet state of the donor or the acceptor has been observed in only a few cases.<sup>13–17</sup> Previous work from this laboratory demonstrated the first donor–acceptor molecule, MeOAn–6ANI–Me<sub>2</sub>Ph–NI, Chart 1, which closely mimics the spin-dependent CR dynamics within the photosynthetic reaction center.<sup>13,14</sup> Transient absorption spectroscopy in toluene determined that excitation of the 6ANI chromophore results in stepwise CS: MeOAn–<sup>1</sup>\*6ANI–Me<sub>2</sub>Ph–NI → <sup>1</sup>[MeOAn<sup>+</sup>–6ANI<sup>–</sup>–Me<sub>2</sub>Ph–NI] → <sup>1</sup>[MeOAn<sup>+</sup>–6ANI–Me<sub>2</sub>Ph–NI<sup>–</sup>] to form the final radical pair with a quantum yield

**Chart 1**

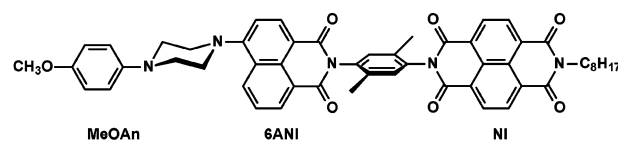
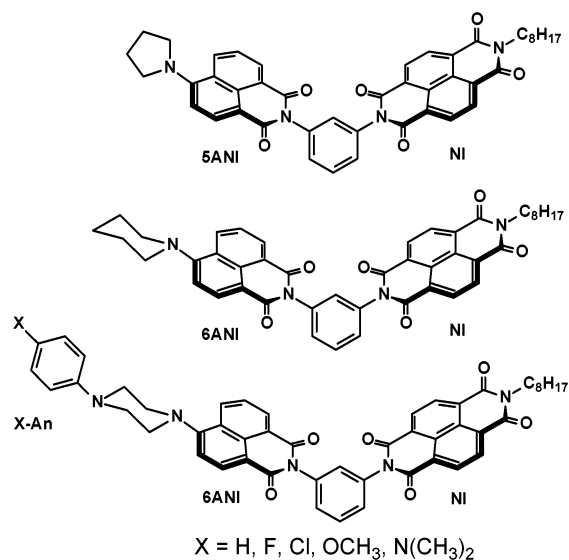


**Chart 2**



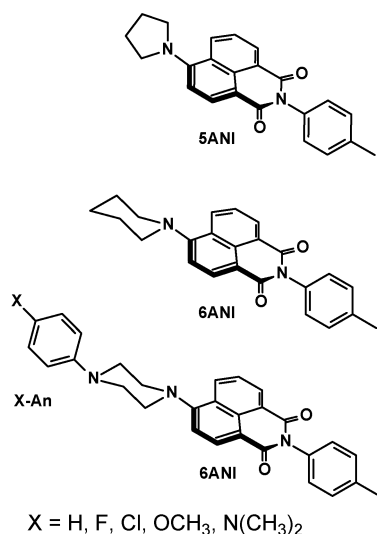
of 0.92. This radical ion pair undergoes RP-ISC to yield  $^3[MeOAn^+-6ANI-Me_2Ph-NI^-]$ , which recombines to give a high yield of MeOAn–6ANI–Me<sub>2</sub>Ph–<sup>3</sup>\*NI. The sublevels of this localized triplet state have unique non-Boltzmann spin populations, which result in spin-polarized EPR spectra that can be detected using time-resolved EPR spectroscopy (TREPR), which closely mimic that observed for photosynthetic reaction centers.<sup>18–21</sup> Subsequently, Gust and co-workers studied a donor–acceptor triad based on a chromophoric porphyrin donor coupled to a fullerene electron acceptor and carotenoid secondary donor that also displays the TREPR spin polarization pattern characteristic of RP-ISC.<sup>15</sup> They also showed that its CR rate was decreased by 50% in the presence of a relatively weak magnetic field ( $B = 0.041$  T).<sup>22</sup> The spin dynamics of radical ion pair recombination on the picosecond scale has also been controlled using applied magnetic fields of several tesla in ferrocene complexes.<sup>23</sup> Up until now there have been no investigations into magnetic field effects on radical ion pairs and their products within a series of structurally rigid intramolecular D–A compounds.

We now present data on a family of closely related rigid donor–acceptor dyads and triads, Chart 2. In the dyads the chromophoric electron donors are 4-(*N*-pyrrolidinyl) and 4-(*N*-piperidinyl)naphthalene-1,8-dicarboximide, 5ANI and 6ANI, respectively, in which the imide groups are linked in a *meta*

- (7) Ogrodnik, A.; Michel-Beyerle, M. E. *Z. Naturforsch.* **1989**, *44a*, 763–764.  
 (8) DiMugno, T. J.; Norris, J. R. In *The Photosynthetic Reaction Center*; Deisenhofer, J., Norris, J. R., Eds.; Academic Press: San Diego, 1993; Vol. 2, pp 105–133.  
 (9) Sumi, H.; Kakitani, T. *Chem. Phys. Lett.* **1996**, *252*, 85–93.  
 (10) Plato, M.; Mobius, K.; Michel-Beyerle, M. E.; Bixon, M.; Jortner, J. *J. Am. Chem. Soc.* **1988**, *110*, 7279–7285.  
 (11) Holzapfel, W.; Finkel, U.; Kaiser, W.; Oesterheld, D.; Scheer, H.; Stülz, H. U.; Zinth, W. *Chem. Phys. Lett.* **1989**, *160*, 1–7.  
 (12) Blankenship, R. E.; Schaafsma, T. J.; Parson, W. W. *Biochim. Biophys. Acta* **1977**, *461*, 297–305.  
 (13) Hasharoni, K.; Levanon, H.; Greenfield, S. R.; Gosztola, D. J.; Svec, W. A.; Wasielewski, M. R. *J. Am. Chem. Soc.* **1995**, *117*, 8055–8056.  
 (14) Hasharoni, K.; Levanon, H.; Greenfield, S. R.; Gosztola, D. J.; Svec, W. A.; Wasielewski, M. R. *J. Am. Chem. Soc.* **1996**, *118*, 10228–10235.  
 (15) Carbonera, D.; Di Valentini, M.; Corvaja, C.; Agostini, G.; Giacometti, G.; Liddell, P. A.; Kuciauskas, D.; Moore, A. L.; Moore, T. A.; Gust, D. *J. Am. Chem. Soc.* **1998**, *120*, 4398–4405.  
 (16) Wiederrecht, G. P.; Svec, W. A.; Wasielewski, M. R. *J. Am. Chem. Soc.* **1999**, *121*, 7726–7727.  
 (17) Wiederrecht, G. P.; Svec, W. A.; Wasielewski, M. R.; Galili, T.; Levanon, H. *J. Am. Chem. Soc.* **2000**, *122*, 9715–9722.

- (18) Thurnauer, M. C.; Katz, J. J.; Norris, J. R. *Proc. Natl. Acad. Sci. U.S.A.* **1975**, *72*, 3270.  
 (19) Dutton, P. L.; Leigh, J. S.; Seibert, M. *Biochem. Biophys. Res. Commun.* **1972**, *46*, 406.  
 (20) Regev, A.; Nechushtai, R.; Levanon, H.; Thornber, J. P. *J. Phys. Chem.* **1989**, *93*, 2421.  
 (21) Rutherford, A. W.; Paterson, D. R.; Mullet, J. E. *Biochim. Biophys. Acta* **1981**, *635*, 205.  
 (22) Kuciauskas, D.; Liddell, P. A.; Moore, A. L.; Moore, T. A.; Gust, D. *J. Am. Chem. Soc.* **1998**, *120*, 10880–10886.  
 (23) Gilch, P.; Pollinger-Dammer, F.; Mueswald, C.; Michel-Beyerle, M. E.; Steiner, U. E. *Science* **1998**, *281*, 982–984.

Chart 3



relationship to a phenyl spacer to which a naphthalene-1,8:4,5-bis(dicarboximide) (NI) electron acceptor is attached. In the triads the same structure is used, except that a 4-(*N*-piperazinyl)-naphthalene-1,8-dicarboximide serves as a chromophoric electron acceptor, the primary donor is a *para*-*X*-aniline (XAn), in which X = H, F, Cl, MeO, and Me<sub>2</sub>N are attached to the *N'* nitrogen of the piperazine, and the secondary acceptor is NI. The dyads and triads undergo photoinduced electron transfer to yield the respective 5ANI<sup>+</sup>–Ph–NI<sup>–</sup>, 6ANI<sup>+</sup>–Ph–NI<sup>–</sup>, and XAn<sup>+</sup>–6ANI–Ph–NI<sup>–</sup> radical ion pair states. These radical ion pairs undergo RP-ISC before recombining to yield <sup>3</sup>\*NI. Application of a 0–1 T external magnetic field prior to photoexcitation results in Zeeman splitting of the triplet sublevels, which produces a decrease in the triplet yield if  $2J$  is small, or a resonance if  $2J$  is somewhat larger, due to enhanced singlet–triplet mixing for fields at which level crossing occurs, Figure 1. The structural rigidity of these compounds permits direct measurement of well-defined  $2J$  resonances. Within the dyads, resonances are observed at field strengths of several tenths of a tesla, while resonances within the triads are observed at much smaller fields. The energy of the  $2J$  resonance correlates strongly with the distance separating the radical ion pairs,  $r_{DA}$ , which relates directly to the electronic coupling matrix element for CR,  $V_{DA}$ .<sup>24–29</sup> In addition,  $2J$  is sensitive to the geometry of the bonding network joining the radical ion pairs, thus making it possible to evaluate the dependence of  $V_{DA}$ , and thus electron transfer rates on the details of the radical ion pair molecular structure.

### Experimental Section

The syntheses of 6ANI–Ph–NI, 6ANI, HAn–6ANI, and MeOAn–6ANI have been reported previously,<sup>30,31</sup> while those of the remaining molecules follow similar procedures and are reported in the Supporting

Information. Characterization was performed with a Gemini 300 MHz, Varian 400 MHz, or INOVA 500 MHz NMR and a PE BioSystems MALDI-TOF mass spectrometer. All solvents were spectrophotometric grade or distilled prior to use.

Cyclic voltammetry measurements were performed in butyronitrile solution containing 0.1 M tetra-*n*-butylammonium perchlorate electrolyte using a CH Model 622 electrochemical workstation. A 1.0 mm diameter platinum disk electrode, platinum wire counter electrode, and Ag/Ag<sub>2</sub>O reference electrode were employed. The ferrocene/ferrocinium couple (Fc/Fc<sup>+</sup>, 0.52 vs SCE) was used as an internal reference for all measurements.

Absorption measurements were made on a Shimadzu (UV-1601) spectrophotometer. The optical density of all samples was maintained between 0.7 and 1.0 at 416 nm ( $\epsilon_{6ANI,416nm} = 7000 \text{ cm}^{-1} \text{ M}^{-1}$ ). Femtosecond transient absorption measurements were made using the 420 nm frequency-doubled output from a regeneratively amplified titanium sapphire laser system operating at 2 kHz as the excitation pulse.<sup>30</sup> Samples were placed in a 2 mm path length quartz cuvette and stirred using a motorized wire stirrer. Nanosecond transient absorption measurements were made using the 416 nm, H<sub>2</sub>-Raman shifted output from a frequency-tripled 10 Hz Nd:YAG laser (QuantaRay DCR-2). Samples were placed in a 10 mm path length quartz cuvette equipped with a vacuum adapter and subjected to five freeze–pump–thaw degassing cycles prior to transient absorption measurements. The probe light in the nanosecond experiments was generated using a xenon flashlamp (EG&G Electro-Optics FX-200) and detected using a photomultiplier tube with high voltage applied to only 4 dynodes (Hamamatsu R928). The total instrument response is 7 ns and is determined primarily by the laser pulse duration. The sample cuvette was placed between the poles of a Walker Scientific HV-4W electromagnet powered by a Walker Magnion HS-735 power supply. The field strength was measured by a Lakeshore 450 gaussmeter with a Hall effect probe. Both the electromagnet and the gaussmeter were interfaced with the data collection computer, allowing measurement and control of the magnetic field to  $\pm 1 \times 10^{-5}$  T during data acquisition.

Kinetic traces were recorded over a range of 2  $\mu$ s. Thirty shots were averaged at each magnetic field strength with a LeCroy 9384 digital oscilloscope and sent to a computer, which calculated the  $\Delta A$ . The relative triplet yield reported is

$$\frac{T}{T_0} = \frac{\Delta A(B)}{\Delta A(B=0)} \quad (1)$$

The results presented are an average of three experiments conducted on separate days with freshly prepared samples.

### Results

**Steady State Spectroscopy.** The photophysics of the 5ANI and 6ANI chromophores have been characterized previously in detail.<sup>31,32</sup> Briefly, their ground state optical spectra exhibit broad charge transfer (CT) absorptions centered at 438 and 397 nm in toluene, respectively. Figure 2 displays the ground state electronic spectra of 5ANI–Ph–NI, 6ANI, and 6ANI–Ph–NI in toluene. The 5ANI and 6ANI CT absorption bands are apparent as well as the vibronic structure (343, 363, and 382 nm) arising from a  $\pi$ – $\pi^*$  transition within the NI acceptor. The spectra of the triads (not shown) are virtually identical to that of 6ANI–Ph–NI, because the *p*-*X*-aniline (X = H, F, Cl, MeO, and Me<sub>2</sub>N) electron donors do not absorb significantly in the visible region of the spectrum.

- (24) Anderson, P. W. *Phys. Rev.* **1959**, *115*, 2–13.  
 (25) Soos, Z. *Annu. Rev. Phys. Chem.* **1974**, *25*, 121–153.  
 (26) Okamura, M. Y.; Isaacson, R. A.; Feher, G. *Biochim. Biophys. Acta* **1979**, *546*, 394.  
 (27) Nelsen, S. F.; Ismagilov, R. F.; Teki, Y. *J. Am. Chem. Soc.* **1998**, *120*, 2200–2201.  
 (28) Kobori, Y.; Sekiguchi, S.; Akiyama, K.; Tero-Kubota, S. *J. Phys. Chem. A* **1999**, *103*, 5416–5424.  
 (29) Yago, T.; Kobori, Y.; Akiyama, K.; Tero-Kubota, S. *J. Phys. Chem. B* **2002**, *106*, 10074–10081.  
 (30) Lukas, A. S.; Miller, S. E.; Wasielewski, M. R. *J. Phys. Chem. B* **2000**, *104*, 931–940.

- (31) Greenfield, S. R.; Svec, W. A.; Gosztoła, D.; Wasielewski, M. R. *J. Am. Chem. Soc.* **1996**, *118*, 6767–6777.  
 (32) Debreczeny, M. P.; Svec, W. A.; Wasielewski, M. R. *New J. Chem.* **1996**, *20*, 815–828.

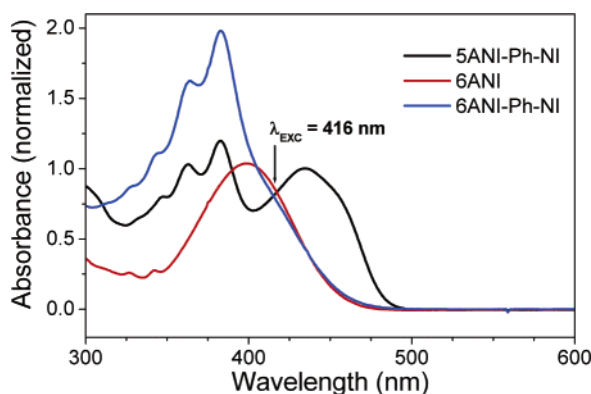


**Figure 2.** Ground electronic spectra of compounds 5ANI-Ph-NI, 6ANI, and 6ANI-Ph-NI in toluene.

**Table 1.** Steady State Photophysical Properties of the Indicated Compounds in Toluene

compound	$\lambda_{\text{ABS}}$ (nm)	$\lambda_{\text{EM}}$ (nm)	$\Phi_{\text{F}}$
5ANI	438	502	0.92
6ANI	397	497	0.91
5ANI-Ph-NI	438	502	0.009
6ANI-Ph-NI	400	498	0.014
An-6ANI	399	517 <sup>a</sup>	0.48 <sup>a</sup>
FAn-6ANI	399	510 <sup>a</sup>	0.62 <sup>a</sup>
ClAn-6ANI	399	510 <sup>a</sup>	0.55 <sup>a</sup>
MeOAn-6ANI	390	572 <sup>a</sup>	0.035 <sup>a</sup>
Me <sub>2</sub> NAn-6ANI	399	>600 <sup>a</sup>	<0.001 <sup>a</sup>
An-6ANI-Ph-NI	399	517 <sup>a</sup>	0.012 <sup>a</sup>
ClAn-6ANI-Ph-NI	399	510 <sup>a</sup>	0.013 <sup>a</sup>
FAn-6ANI-Ph-NI	399	510 <sup>a</sup>	0.014 <sup>a</sup>
MeOAn-6ANI-Ph-NI	390	570 <sup>a</sup>	0.002 <sup>a</sup>
Me <sub>2</sub> NAn-6ANI-Ph-NI	399	>600 <sup>a</sup>	<0.001 <sup>a</sup>

<sup>a</sup> Fluorescence resulting from charge recombination.

The <sup>1</sup>\*5ANI and <sup>1</sup>\*6ANI states can act as either electron donors or acceptors. Attachment of the NI electron acceptor via a *meta*-substituted phenyl bridge to either 5ANI or 6ANI results in nearly complete quenching of their fluorescence in toluene, as reflected in the steady state quantum yield data listed in Table 1 and suggesting that the 5ANI<sup>+</sup>-Ph-NI<sup>-</sup> and 6ANI<sup>+</sup>-Ph-NI<sup>-</sup> radical ion pairs are formed with quantum yields exceeding 0.98 (see below). Reference compounds XAn-6ANI, where X = H, F, Cl, MeO, and Me<sub>2</sub>N, have the *para*-substituted electron donors attached to 6ANI via a piperazine bridge as shown in Chart 3. The fluorescence quantum yields from <sup>1</sup>\*6ANI in these molecules are all < 0.003, while the radical ion pair states XAn<sup>+</sup>-6ANI<sup>-</sup> all undergo radiative recombination to ground state, except when X = N(CH<sub>3</sub>)<sub>2</sub>. The radiative recombination makes it possible to accurately assess the free energy for the reaction XAn-6ANI → XAn<sup>+</sup>-6ANI<sup>-</sup>.<sup>31</sup>

**Redox Potentials.** The electrochemical properties of aromatic imide and diimide chromophores are highly sensitive to the nature of the imide substituent.<sup>33</sup> The 5ANI and 6ANI chromophores undergo reversible oxidation and reduction at modest potentials, as indicated by cyclic voltammetry. The redox potentials for all the molecules used in this study are given in Table 2. The oxidation potentials of 5ANI and 6ANI (1.06 and 1.23 V, respectively) are very similar to the oxidation potentials of *N*-methylpyrrolidine and *N*-methylpiperidine, respectively, while their reduction potentials are both about -1.3 V and

**Table 2.** Redox Potentials of the Indicated Compounds Measured in Butyronitrile Containing 0.1 M Tetra-*n*-butylammonium Perchlorate<sup>a</sup>

compound	XAn <sup>+</sup>	ANI <sup>-1</sup>	ANI <sup>-1</sup>	NI <sup>-1</sup>
5ANI-Ph-NI		1.06	-1.30	-0.49
6ANI-Ph-NI		1.23	-1.32	-0.49
An-6ANI-Ph-NI	1.02	1.25	-1.31	-0.50
ClAn-6ANI-Ph-NI	1.12	1.40	-1.30	-0.49
FAn-6ANI-Ph-NI	1.07	1.20	-1.31	-0.49
MeOAn-6ANI-Ph-NI	0.82	1.22	-1.30	-0.50
Me <sub>2</sub> NAn-6ANI-Ph-NI	0.33	1.31	-1.29	-0.49

<sup>a</sup> All potentials versus saturated calomel electrode (SCE).

correspond closely to that of naphthalene-1,8-dicarboximide. The first reduction potential of NI occurs at -0.5 V and is constant within the series of dyad and triad compounds. The oxidation potentials of the HAn, FAn, ClAn, MeOAn, and Me<sub>2</sub>NAn electron donors correlate strongly with the electron-withdrawing or -releasing nature of the *para* substituent attached to the aniline. Only MeOAn and Me<sub>2</sub>NAn have oxidation potentials substantially less positive than that of 6ANI.

**Time-Resolved Charge Separation Dynamics.** Transient absorption spectroscopy permits direct observation of the intermediates formed via photoinduced electron transfer. The CS rates were measured after excitation of the 5ANI or 6ANI chromophores with a 416 nm, 130 fs laser flash. The presence of NI within 5ANI-Ph-NI and 6ANI-Ph-NI results in rapid CS to form the 5ANI<sup>+</sup>-Ph-NI<sup>-</sup> and 6ANI<sup>+</sup>-Ph-NI<sup>-</sup> radical ion pairs, respectively. These are detected by the presence of the NI<sup>-</sup> radical anion, which has distinct absorptions at 480 nm ( $\epsilon = 28\,300\text{ cm}^{-1}\text{ M}^{-1}$ ) and 605 nm ( $\epsilon = 7000\text{ cm}^{-1}\text{ M}^{-1}$ ), as shown in Figure 3A.<sup>34</sup> The time constants for CS are listed in Table 3. Analogously, attachment of electron donors to the 6ANI chromophore within the reference molecules given in Chart 3 results in electron transfer to form the XAn<sup>+</sup>-6ANI<sup>-</sup> radical pairs, as detected by the presence of the 6ANI<sup>-</sup> radical, which has distinct absorptions at 420 nm ( $\epsilon = 23\,500\text{ cm}^{-1}\text{ M}^{-1}$ ) and 510 nm ( $\epsilon = 7000\text{ cm}^{-1}\text{ M}^{-1}$ ), as well as by monitoring the formation and decay of stimulated emission resulting from radiative ion pair recombination. The time constants for photoinduced electron transfer are listed in Table 3 and show that the reaction XAn-6ANI → XAn<sup>+</sup>-6ANI<sup>-</sup> is very rapid for all substituents X.

Within the triads the reaction XAn-<sup>1</sup>\*6ANI-Ph-NI → XAn<sup>+</sup>-6ANI<sup>-</sup>-Ph-NI is much faster than the corresponding reaction XAn-<sup>1</sup>\*6ANI-Ph-NI → XAn-6ANI<sup>+</sup>-Ph-NI<sup>-</sup>, so that the overall formation of the distal radical ion pair occurs by the reaction sequence XAn-<sup>1</sup>\*6ANI-Ph-NI → XAn<sup>+</sup>-6ANI<sup>-</sup>-Ph-NI → XAn<sup>+</sup>-6ANI-Ph-NI<sup>-</sup>. The rate constants and free energies<sup>31</sup> for these reactions are given in Table 3. For example, within MeOAn-6ANI-Ph-NI the primary CS event is formation of the MeOAn<sup>+</sup>-6ANI<sup>-</sup>-Ph-NI ion pair, as measured by the appearance of the 510 nm absorption band of 6ANI<sup>-</sup>, as seen in the transient spectra of MeOAn-6ANI-Ph-NI at early times within Figure 3B. The 510 nm 6ANI<sup>-</sup> peak disappears with a time constant of 120 ps, which is identical to that for the appearance of the NI<sup>-</sup> peaks at 480 and 610 nm. This distal radical ion pair is formed with a quantum yield in excess of 0.99.

(33) Viehbeck, A.; Goldberg, M. J.; Kovac, C. A. *J. Electrochem. Soc.* **1990**, *137*, 1460–1466.

(34) Wiederrecht, G. P.; Niemczyk, M. P.; Svec, W. A.; Wasielewski, M. R. *J. Am. Chem. Soc.* **1996**, *118*, 81–88.

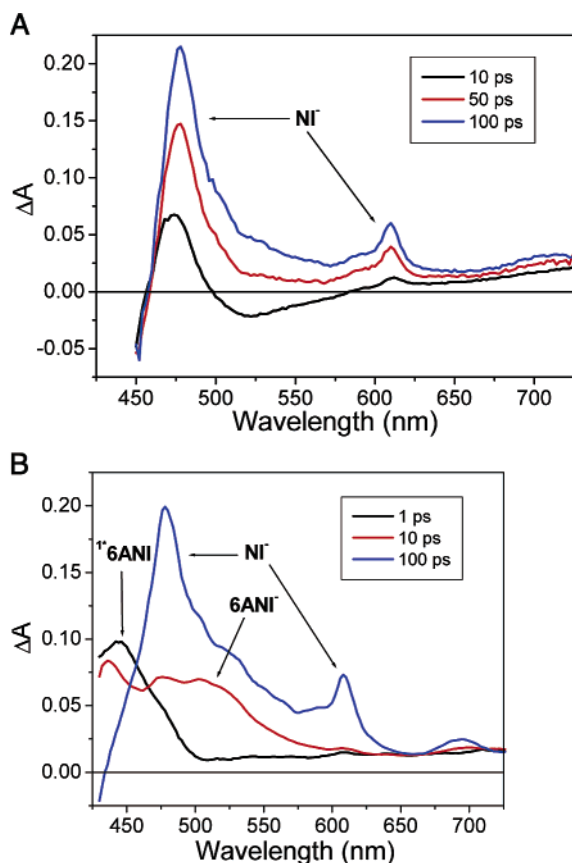


**Figure 3.** (A) Transient absorption spectra of 6ANI–Ph–NI at the times indicated following excitation with a 420 nm, 130 fs laser flash. (B) Transient absorption spectra of MeOAn–6ANI–Ph–NI at the times indicated following excitation with a 420 nm, 130 fs laser flash.

**Charge Recombination in the Absence of an External Magnetic Field.** The transient absorption spectra of MeOAn–6ANI–Ph–NI following excitation with a 416 nm, 7 ns laser flash are displayed in Figure 4. At early times ( $t = 60$  ns), the spectrum displays sharp features at 480 and 605 nm characteristic of the MeOAn<sup>+</sup>–6ANI–Ph–NI<sup>–</sup> radical ion pair. While the transient absorption spectra of the singlet and triplet radical ion pair states are indistinguishable from one another, they undergo CR via different pathways. The singlet radical ion pair recombines to ground state, which is the baseline within the transient absorption experiment, while the triplet radical ion pair recombines to form the neutral triplet state. The spectrum at longer times ( $t = 600$  ns) within Figure 4 arises from <sup>3\*</sup>[MeOAn–6ANI–Ph–NI]. TREPR has shown that this triplet state is localized on NI within analogous dyads and triads.<sup>13</sup> Therefore the broad absorption centered at 480 nm in the transient spectrum is due to MeOAn–6ANI–Ph–<sup>3\*</sup>NI. These CR dynamics give rise to transient kinetics at 480 nm, which are characterized by an instrument-limited rise followed by exponential decay to a shelf, as seen in the inset to Figure 4. The rate constants for CR at  $B = 0$  T are a sum of the rates for CR of the singlet and triplet radical ion pairs, labeled within Figure 5 as  $k_S$  and  $k_T$ , respectively. These rate constants most likely differ considerably due to large differences in the free energies of reaction.

**Charge Recombination in the Presence of a Magnetic Field.** The amplitude of the long-lived component within the transient kinetics directly measures the XAn–6ANI–Ph–<sup>3\*</sup>NI

population. TREPR measurements on closely related compounds have shown that the triplet levels of the radical ion pair are higher in energy than that of the singlet state, which makes  $2J$  negative within this series of compounds.<sup>13</sup> According to the Heitler–London model, the singlet radical pair is stabilized while the triplet is destabilized.<sup>35</sup> Having noted this fact, for convenience we will ignore the sign of  $2J$  in our subsequent discussion. At zero field, the degree of mixing of the singlet and triplet radical pair states is determined by  $2J$  and the electron–nuclear hyperfine interactions within each radical. Application of an external magnetic field splits the triplet sublevels into  $T_{\pm 1}$  and  $T_0$  levels via the Zeeman interaction, as shown in Figure 1. As the field increases, the  $T_{-1}$  sublevel comes into resonance with  $S$ , which leads to increased  $S \leftrightarrow T_{-1}$  mixing. While absolute changes in the singlet and triplet sublevel populations cannot be detected using magnetic fields alone, the increased mixing of the spin states at the level crossing increases the yield of <sup>3\*</sup>NI formed from CR of the triplet radical pair, which is detected by transient absorption. Further increases in the magnetic field strength increase the  $S$ – $T_{-1}$  energy gap, which results in a decrease in the triplet yield to a constant value that is due to  $S$ – $T_0$  mixing alone. The overall effect is observed as an increase in the triplet product of charge recombination when the  $S$ – $T_{-1}$  resonance condition is satisfied, followed by a decrease when  $S$  can only interact with  $T_0$ .<sup>36,37</sup> Thus by observing the change in population of the neutral localized triplet state as a function of magnetic field we have a sensitive direct gauge of the singlet–triplet energy difference,  $2J$ , within the radical ion pair.

The production of <sup>3\*</sup>NI (formed via RP-ISC) as a function of external magnetic field strength (0–1 T) within 5ANI–Ph–NI, 6ANI–Ph–NI, and the triads is shown in Figures 6, 7A, and 7B. Each of these compounds displays a distinct resonance at  $2J$ . The values of  $2J$  are determined from these plots and are listed in Table 4. The CR time constants at zero field,  $2J$ , and 1 T are also given in Table 4.

## Discussion

**Theory.** The formation of triplet states within 5ANI–Ph–NI, 6ANI–Ph–NI, and XAn–6ANI–Ph–NI occurs via the RP-ISC mechanism. This mechanism can be described by the spin-Hamiltonian

$$H_{ST} = \beta B_0 (g_1 \mathbf{S}_1 + g_2 \mathbf{S}_2) + \sum_i a_{1i} \mathbf{S}_1 \cdot \mathbf{I}_i + \sum_k a_{2k} \mathbf{S}_2 \cdot \mathbf{I}_k - J(\mathbf{I}_1 \cdot \mathbf{I}_2) + 2\mathbf{S}_1 \cdot \mathbf{S}_2 \quad (2)$$

where  $\beta$  is the Bohr magneton,  $B_0$  is the applied magnetic field,  $g_1$  and  $g_2$  are the electronic  $g$ -factors for each radical,  $\mathbf{S}_1$  and  $\mathbf{S}_2$  are electron spin operators for the two radicals within the radical pair,  $\mathbf{I}_i$  and  $\mathbf{I}_k$  are nuclear spin operators,  $a_{1i}$  and  $a_{2k}$  are the isotropic hyperfine coupling constants of nucleus  $i$  with radical 1 and nucleus  $k$  with radical 2, and  $J$  is the scalar spin–spin exchange interaction constant. Anisotropic exchange interactions, dipolar hyperfine couplings, and the magnetic dipole–dipole interaction are neglected because the measure-

(35) Alexander, M. H.; Salem, L. *J. Chem. Phys.* **1967**, *46*, 430.

(36) Weller, A.; Staerk, H.; Treichel, R. *Faraday Discuss. Chem. Soc.* **1984**, *78*, 271–278.

(37) Weller, A.; Nolting, F.; Staerk, H. *Chem. Phys. Lett.* **1983**, *96*, 24–27.

**Table 3.** Free Energies and Time Constants for Charge Separation and Recombination in Toluene

compound	$\Delta G_{CS1}$ (eV)	CS <sub>1</sub> (ps)	$\Delta G_{CR1}$ (eV)	CR <sub>1</sub> (ns)	$\Delta G_{CS2}$ (eV)	CS <sub>2</sub> (ps)	$\Delta G_{CR2}$ (eV)	CR <sub>2</sub> (ns)
5ANI–Ph–NI	–0.54	85	2.11	45				
6ANI–Ph–NI	–0.53	120	2.27	120				
An–6ANI	–0.08	18	2.72	5.0				
FAn–6ANI	–0.06	28	2.74	5.2				
ClAn–6ANI	–0.06	27	2.74	5.4				
MeOAn–6ANI	–0.32	7.7	2.48	5.3				
Me <sub>2</sub> NAn–6ANI	–0.81	1.2	1.99	0.15				
An–6ANI–Ph–NI	–0.08	18	2.72		–0.19	120	–2.53, <sup>a</sup> –0.48 <sup>b</sup>	120
ClAn–6ANI–Ph–NI	–0.06	30	2.74		–0.10	120	–2.55, <sup>a</sup> –0.50 <sup>b</sup>	112
FAn–6ANI–Ph–NI	–0.06	25	2.74		–0.14	120	–2.60, <sup>a</sup> –0.55 <sup>b</sup>	168
MeOAn–6ANI–Ph–NI	–0.32	8.0	2.48		–0.48	40	–2.00, <sup>a</sup> 0.05 <sup>b</sup>	73
Me <sub>2</sub> NAn–6ANI–Ph–NI	–0.81	1.3	1.99		–0.53	25	–1.46, <sup>a</sup> 0.59 <sup>b</sup>	100

<sup>a</sup> Recombination to ground state. <sup>b</sup> Recombination to NI triplet state.

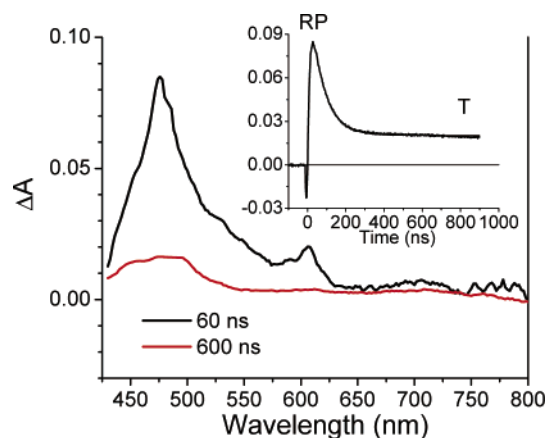


**Figure 4.** Transient absorption spectra of MeOAn–6ANI–Ph–NI at the times indicated following excitation with a 416 nm, 7 ns laser flash. Inset: Kinetics monitoring the 480 nm spectral features.

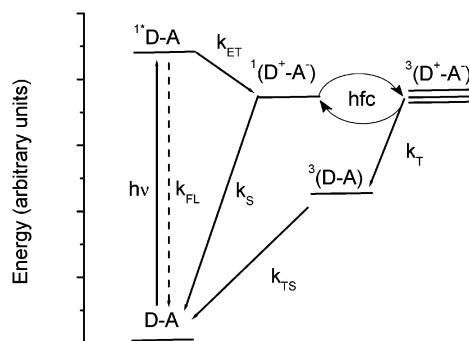


**Figure 5.** Energy level diagram for relevant donor–acceptor electronic states.

ments are performed in solution. Also, it is assumed that nuclei associated structurally with a given radical couple only with the electron spin within that radical.

Zeeman splitting of the triplet sublevels requires an applied magnetic field, and thus the first term in eq 2 cannot contribute to  $S \leftrightarrow T$  mixing at zero field. As the strength of the magnetic field increases, contributions from this term will begin to contribute to  $S \leftrightarrow T$  mixing due to differences in the isotropic  $g$ -factors of the two electron spins. The frequency for conversion of the spins from singlet to triplet is given by eq 3:

$$\Delta\omega = \frac{\Delta g\beta B_0}{\hbar} \quad (3)$$

where  $\Delta g$  is the difference in  $g$ -factors for the two radicals.

The small differences in  $g$ -factors for organic radicals such as those studied here contribute to singlet–triplet mixing only at field strengths of several tesla. There is no experimental evidence within Figures 6 and 7 for a  $\Delta g$  contribution because the data do not show a monotonic increase in triplet product yield as a function of field strength. Therefore, for the range of field strengths in the present study, singlet–triplet mixing of the radical pairs within these compounds is driven largely by the hyperfine and exchange interactions.

In general, hyperfine interactions (HFI) between the magnetic moments of the unpaired electrons and those of nearby nuclei drive singlet–triplet mixing at zero and small magnetic fields.<sup>1–3</sup> Weller and co-workers have shown that for a series of organic radical ion pairs, the magnetic field value at half-saturation due to HFI can be approximated by eq 4:<sup>36,37</sup>

$$B_{1/2} = 2 \left( \frac{B_D^2 + B_A^2}{B_D + B_A} \right) \quad (4)$$

where  $B_D$  and  $B_A$  refer to the energies of the hyperfine interactions between the nuclear spins and unpaired electron spins on the donor and acceptor. These may be determined from the values of the isotropic electron–nuclear hyperfine coupling constants  $a_{ik}$  for the nuclear spins  $I_k$  on radical  $i$  using eq 5:

$$B_i = \left[ \sum_k I_k(I_k + 1)a_{ik}^2 \right]^{1/2} \quad (5)$$

The values of  $a_{ik}$  for  $\text{NI}^-$  and  $\text{MeOAn}^+$ , as well as those for the radical cations of  $N$ -methylpyrrolidine and  $N$ -methylpiperidine, were obtained from the literature.<sup>38–40</sup> The values of  $a_{ik}$  for  $\text{XAn}^+$  ( $X = \text{H}, \text{Cl}, \text{F}$ ) were obtained by scaling their calculated spin densities given in Table 5 using the calculated and experimental hyperfine couplings observed for  $\text{MeOAn}^+$ . Values of  $B_{1/2}$  for  $5\text{ANI}^+-\text{Ph}-\text{NI}^-$ ,  $6\text{ANI}^+-\text{Ph}-\text{NI}^-$ , and  $\text{XAn}^+-6\text{ANI}-\text{Ph}-\text{NI}^-$  were calculated using these hyperfine coupling constants and eqs 4 and 5 and are listed in Table 4. For compounds that display distinct resonances,  $B_{1/2} \cong (1/2)\Delta B$ , where  $\Delta B$  is the full width at half-maximum of the resonance.

The exchange interaction,  $2J$ , is defined as the energy splitting between the singlet and triplet radical pairs and likely arises

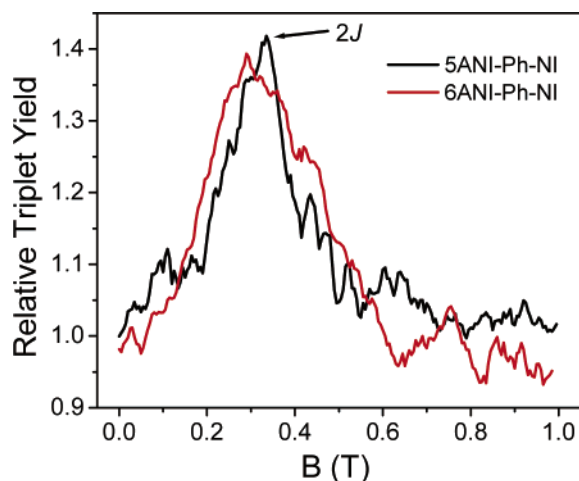
(38) Zhong, C. J.; Kwan, W. S. V.; Miller, L. L. *Chem. Mater.* **1992**, *4*, 1423–1428.

(39) Ciminale, F.; Curci, R.; Portacci, M.; Troisi, L. *Tetrahedron Lett.* **1988**, *29*, 2463–2466.

(40) Eastland, G. W.; Rao, D. N. R.; Symons, M. C. R. *J. Chem. Soc., Perkin Trans. 2* **1984**, 1551–1557.

**Table 4.** Experimentally Determined Values for  $2J$ ,  $B_{1/2}$  and Charge Recombination Rates at  $B = 0$  G,  $2J$ , and 1 T, and  $B_{1/2}$  Values Calculated Using Eqs 4 and 5 from HFI Literature Values<sup>38–40</sup>

	$2J$ (mT)	$B_{1/2}$ (mT) exptl	$B_{1/2}$ (mT) calc	T(0)/RP	$\tau_{CR}$ (ns) $B = 0$ T	$\tau_{CR}$ (ns) $B = 2J$	$\tau_{CR}$ (ns) $B = 1$ T
5ANI–Ph–NI	305	80	4.2	0.12	45	42	45
6ANI–Ph–NI	320	130	4.2	0.09	120	107	120
An–6ANI–Ph–NI	52.5	72.5	3.9	0.24	120	96	153
CIAn–6ANI–Ph–NI	32.5	102.5	3.9	0.31	112	100	177
FAn–6ANI–Ph–NI	60.0	123	4.2	0.26	168	138	214
MeOAn–6ANI–Ph–NI	1.5	2.2	3.8	0.25	73	84	68
	15.0	3.0					
Me <sub>2</sub> NAn–6ANI–Ph–NI			3.9		100		100

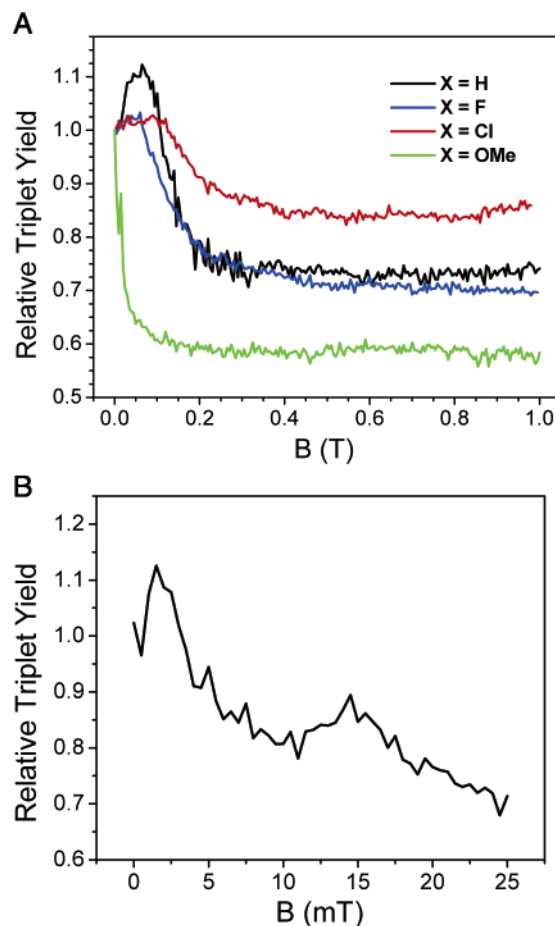
**Figure 6.** Relative triplet yield for the indicated dyads at 0–1 T.

from interactions between the frontier orbitals of the radical pairs. Figure 1 shows that the Zeeman splitting of the triplet sublevels causes  $S \leftrightarrow T_{-1}$  level crossing when  $B = 2J$ , which leads to the maximum in the triplet product yields observed in Figures 6 and 7. At higher field strengths only  $S \leftrightarrow T_0$  mixing occurs, at which point the magnetic field effect saturates. Weller relates the observed resonance at  $B = 2J$  to  $r_{DA}$  using

$$2J(r) = 2J_0 e^{-\alpha(r_{DA} - r_0)} \quad (6)$$

where  $2J(r)$  is obtained from the peak of the observed resonance,  $r_{DA}$  is the radical ion pair separation,  $r_0$  is the van der Waals contact distance of 3.4 Å, and  $2J_0$  and  $\alpha$  are constants. The preexponential  $2J_0$  includes the dependence of the spin–spin exchange interaction on the geometry of the radical pair. Equation 6 predicts that the observed resonance should move to lower fields as the distance between the radical ions increases.

**Magnetic Field Effects on Charge Recombination within the Dyads and Triads.** The two dyads, 5ANI–Ph–NI and 6ANI–Ph–NI, which differ only in the number of carbon atoms in the cyclic amine of the chromophore, display broad  $2J$  resonances near 0.3 T, Figure 6. Likewise, the calculated  $B_{1/2}$  values are virtually identical for these compounds, Table 4. However, comparison of the experimental and calculated  $B_{1/2}$  values shows that the observed  $B_{1/2}$  values are 1 to 2 orders of magnitude larger than those calculated assuming a contribution from HFI alone. Given that the measured lifetimes of 5ANI<sup>+</sup>–Ph–NI<sup>−</sup> and 6ANI<sup>+</sup>–Ph–NI<sup>−</sup> are never less than 42 ns at 0–1 T, Table 4, the line widths of their  $2J$  resonances are not due to uncertainty broadening ( $\hbar = 5.7 \times 10^{-12}$  T·s).<sup>41</sup> Thus, within

**Figure 7.** (A) Relative triplet yields for XAn–6ANI–Ph–NI triads at 0–1 T. (B) Relative triplet yield for MeOAn–6ANI–Ph–NI at 0–25 mT.

5ANI<sup>+</sup>–Ph–NI<sup>−</sup> and 6ANI<sup>+</sup>–Ph–NI<sup>−</sup> the spin Hamiltonian (eq 2) is dominated by the exchange interaction,  $2J$ , and the assumption can be made that  $2J \gg E_{\text{HFI}}$ .

The triads are structurally similar to the dyads, but exhibit smaller  $2J$  values and much sharper resonances. This is due to delocalization of charge and spin density away from 6ANI toward the HAn, FAn, CIAn, and MeOAn electron donors within the triads and increases the radical ion pair distance relative to that in 6ANI–Ph–NI depending on the oxidation potential of XAn. In MeOAn<sup>+</sup>–6ANI–Ph–NI<sup>−</sup>, the observed  $B_{1/2}$  values agree very well with those calculated from the HFI using eqs 4 and 5. The fact that  $2J \approx E_{\text{HFI}}$  implies that the HFI plays a significant role in  $S \leftrightarrow T$  mixing at zero field within MeOAn<sup>+</sup>–6ANI–Ph–NI<sup>−</sup>. In the triads where X = H, F, and Cl the observed values of  $B_{1/2}$  are over an order of magnitude larger than the calculated values, so that  $2J \gg E_{\text{HFI}}$ , as is ob-

(41) Staerk, H.; Treichel, R.; Weller, A. *Chem. Phys. Lett.* **1983**, *96*, 28–30.

**Table 5.** Calculated Spin Densities for the Cation Radicals of 5ANI, 6ANI, and XAn–6ANI, where X = H, F, Cl, MeO, and Me<sub>2</sub>N, Determined Using UHF-AM1 Calculations<sup>a</sup>

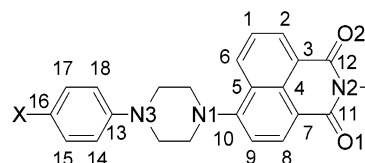
atom	6ANI	5ANI	H	F	Cl	MeO	Me <sub>2</sub> N
C1	0.400	0.385	0.012	0.009	0.008	0.006	0.002
C2	-0.386	-0.367	-0.012	-0.008	-0.007	-0.006	-0.002
C3	0.429	0.420	0.012	0.009	0.008	0.006	0.002
C4	-0.418	-0.412	-0.013	-0.009	-0.008	-0.006	-0.002
C5	0.386	0.366	0.014	0.009	0.009	0.007	0.002
C6	-0.363	-0.334	-0.013	-0.009	-0.008	-0.007	-0.002
C7	0.617	0.644	0.018	0.013	0.012	0.009	0.003
C8	-0.461	-0.457	-0.016	-0.011	-0.011	-0.008	-0.002
C9	0.545	0.551	0.019	0.014	0.013	0.010	0.003
C10	-0.309	-0.261	-0.020	-0.014	-0.014	-0.010	-0.003
C11	-0.079	-0.083	-0.002	-0.001	-0.001	-0.001	-0.000
C12	0.053	0.051	-0.001	-0.001	-0.001	-0.001	-0.000
O1	-0.089	-0.094	-0.003	-0.002	-0.002	-0.001	-0.000
O2	-0.060	-0.059	-0.002	-0.001	-0.001	-0.001	-0.000
N1	0.543	0.454	0.018	0.017	0.017	0.011	0.004
N2	-0.017	-0.018	0.000	0.000	0.000	0.000	0.000
N3			0.609	0.581	0.585	0.528	0.352
C13			-0.280	-0.264	-0.272	-0.151	-0.090
C14			0.468	0.429	0.445	0.350	0.010
C15			-0.396	-0.377	-0.389	-0.264	0.054
C16			0.531	0.498	0.518	0.386	0.066
C17			-0.395	-0.377	-0.389	-0.248	0.055
C18			0.469	0.430	0.446	0.295	-0.009
X			-0.029	-0.060	-0.035	0.096	0.373

<sup>a</sup> Atoms are labeled according to Chart 4.

served for the dyads. The degree of  $S \leftrightarrow T$  mixing at zero field within the radical pair is best illustrated by the ratio of the localized triplet  $^3\text{NI}$  yield to that of the radical ion pair,  $T(0)/\text{RP}$ , as indicated in the Figure 4 inset. The absorption ratios directly reflect the  $T(0)/\text{RP}$  yield ratio and are listed in Table 4. These data show that, as expected, the yield of  $^3\text{NI}$  following charge recombination is much higher within the triads than the dyads.

Given the smaller values of  $2J$  for the triads relative to the dyads, the hyperfine interaction makes a much more significant contribution to  $S \leftrightarrow T$  mixing. At low field it is difficult to separate the contributions of each mechanism in terms of population and depopulation rates of the mixed states. Nevertheless, several observed trends between the CR rates at  $B = 0$  T,  $2J$ , and 1 T should be mentioned. First, it is clear from comparing CR time constants at  $B = 0$  and 1 T that  $S$  most likely interacts with all three triplet sublevels at zero field. As the field increases, the CR time constants become shorter at  $B = 2J$  due to increased  $S \leftrightarrow T_{-1}$  mixing. At higher fields, the time constants for CR become longer again because  $S$  mixes only with  $T_0$ . Interestingly, compound MeOAn–6ANI–Ph–NI is an exception to this trend; its CR time constant is longer when  $B = 2J$  and shorter at high fields. This is a consequence of an additional mechanistic complexity for this molecule. TREPR spectra published earlier show that the emission, absorption spin polarization pattern of the EPR lines observed at early times for the closely related MeOAn<sup>+</sup>–6ANI–Me<sub>2</sub>Ph–NI<sup>-</sup> radical ion pair (Chart 1) is a consequence of its singlet state precursor, MeOAn–<sup>1</sup>6ANI–Me<sub>2</sub>Ph–NI.<sup>13</sup> However, the energies of MeOAn<sup>+</sup>–6ANI–Me<sub>2</sub>Ph–NI<sup>-</sup> and MeOAn–6ANI–Me<sub>2</sub>Ph–<sup>3</sup>NI are nearly degenerate, so that as a function of time an equilibrium between these two states is established, which leads to a significant population of  $^3[\text{MeOAn}^+ - 6\text{ANI} - \text{Me}_2\text{Ph} - \text{NI}^-]$  produced from MeOAn–6ANI–Me<sub>2</sub>Ph–<sup>3</sup>NI. This results in an inversion of the spin polarization pattern as a function of time, indicating that the

**Chart 4**



triplet radical ion pair originated from an excited triplet state. The same mechanism occurs for MeOAn–6ANI–Ph–NI, in which repopulation of the radical ion pair results in the longest CR time constants occurring when  $S \leftrightarrow T_{-1}$  mixing is strongest, i.e., at  $B = 2J$ .

The 4-dimethylaminoaniline (Me<sub>2</sub>NAn) donor within Me<sub>2</sub>NAn–6ANI–Ph–NI undergoes reversible oxidation at 0.33 V vs SCE, the most negative oxidation potential in this series of compounds. This results in rapid CS with  $\tau_{\text{CS1}} = 1.3$  ps and  $\tau_{\text{CS2}} = 25$  ps, forming Me<sub>2</sub>NAn<sup>+</sup>–6ANI–Ph–NI<sup>-</sup> with unity quantum yield. However, no magnetic field effect is observed for this compound because the radical pair can only undergo CR to the singlet ground state since  $\Delta G = 0.59$  eV for  $^3[\text{Me}_2\text{NAn}^+ - 6\text{ANI} - \text{Ph} - \text{NI}^-] \rightarrow [\text{Me}_2\text{NAn} - 6\text{ANI} - \text{Ph} - ^3\text{NI}]$ . While significant  $S \leftrightarrow T$  mixing is likely to occur within the radical pair, no field-dependent change is observed in the CR rate because singlet CR is field independent.

#### Relating $2J$ Resonances to Radical Ion Pair Structure and Electronic Coupling.

An analysis of the relationship between the observed  $2J$  resonances and the structures of the radical ion pairs requires an estimation of the spin densities within the radical ion pairs and the effective distance between the spin distributions within the radical ion pairs,  $r_{\text{DA}}$ . The energy-minimized structures of the cation and anion radicals within the dyads and triads were calculated using the unrestricted Hartree–Fock (UHF) AM1 method.<sup>42</sup> The spin density distribution within the NI<sup>-</sup> radical anion is symmetric and principally resides within the naphthalene ring, so that the geometric center of NI<sup>-</sup> is the center of its spin distribution. The spin densities for selected atoms within the cation radicals are listed in Table 5 according to the nomenclature given in Chart 4. Significant spin density resides on the nitrogen atom (N1) attached to the 4-position of the naphthalene-1,8-dicarboximide ring of 5ANI<sup>+</sup> and 6ANI<sup>+</sup>. In contrast, the largest spin density in each triad resides on the piperazine nitrogen (N3) that is part of XAn. As the electron-releasing MeO and Me<sub>2</sub>N substituents stabilize the positive charge, the spin distribution within XAn<sup>+</sup> shifts away from N3 and toward these substituents. The calculated spin densities suggest that the average distance between the spin density distributions of each radical ion within 6ANI<sup>+</sup>–Ph–NI<sup>-</sup> and 5ANI<sup>+</sup>–Ph–NI<sup>-</sup> should be significantly shorter than the corresponding distances in XAn<sup>+</sup>–6ANI–Ph–NI<sup>-</sup>. A reasonable estimate of the effective radical ion pair distances in these molecules can be obtained using the spin densities to weight the distances between the individual atoms in the radical cation and the center of NI<sup>-</sup> for each molecule. Since the through-bond contribution to the overall electronic coupling between covalently linked radical ion pairs at fixed distances usually dominates, we measure the distances from the individual atoms of the radical cation to the center of the phenyl group attaching it to NI<sup>-</sup> and then add to it the 7.8 Å distance from the center of the phenyl to that of NI<sup>-</sup>. These distances are then

(42) AM1 calculations were performed using HyperChem; Hypercube, Inc., 1115 NW 1114th St., Gainesville, FL 32601.

weighted by the calculated spin densities of the radical cation and summed to yield  $r_{DA}$ . Generally,  $r_{DA}$  increases as the radical cation is stabilized by substituent effects.

The limited degree of conformational freedom within the radical ion pairs studied here means that eq 6 should provide a reasonable description of the dependence of  $2J$  on  $r_{DA}$ . However, comparisons between molecules using eq 6 are valid only if each radical ion pair in the series has the same free energy of formation and recombination. This stems from the fact that the exchange interaction for a radical ion pair is directly related to the electronic coupling matrix elements,  $V_n$ , and the respective energy gaps at its relaxed geometry,  $\Delta E_n$ , between the radical ion pair and the  $n$  states from which it is formed and to which it decays by a relationship derived from second-order perturbation theory:<sup>24–29</sup>

$$2J = \sum_n \frac{V_n^2}{\Delta E_n} \quad (7)$$

Given the much smaller energy gap between the triplet radical ion pair state and the triplet state of NI that results from CR relative to that between the singlet radical ion pair state and singlet ground state for each molecule, Table 3, we assume that the term in eq 7 that couples the triplet radical ion pair state to the triplet recombination product dominates, so that

$$2J = -\frac{V_{\text{CRT}}^2}{\Delta G_{\text{CRT}} + \lambda} \quad (8)$$

where  $\lambda$  is the vertical reorganization energy for CR within the radical ion pair leading to the local neutral triplet state of NI and  $\Delta G_{\text{CRT}} = E(\text{triplet}) - E(\text{radical ion pair})$ . The total reorganization energy  $\lambda = \lambda_S + \lambda_I$ , where  $\lambda_S$  is the contribution from the solvent and  $\lambda_I$  is the internal structural reorganization of the donor and acceptor. Noting that the static and high-frequency dielectric constants of toluene are almost equal, the Marcus dielectric continuum model<sup>43</sup> predicts that  $\lambda_S$  is negligible. The value of  $\lambda_I$  typically assigned to aromatic donors and acceptors is 0.3 eV,<sup>44</sup> so that  $\lambda = 0.3$  eV.

The term  $\alpha$  in eq 6 can be directly related to the exponential damping factor  $\beta$  for the distance dependence of the rate constant for nonadiabatic electron transfer.<sup>45–47</sup> Since the semiclassical Marcus–Jortner theory of electron transfer shows that the rate of electron transfer  $k_{\text{ET}} \propto V^2$ , eq 8 implies that  $k_{\text{CRT}} \propto 2J$ . Thus, the exponential damping factor  $\alpha$  for the distance dependence of  $2J$  (eq 6) should be equal to  $\beta$ , the comparable factor for the distance dependence of the charge recombination rate. Plotting  $\ln(2J(\Delta G_{\text{CRT}} + \lambda))$  vs  $r_{DA}$  in Figure 8 results in a best-fit line with slope  $\alpha = 0.5 \pm 0.1 \text{ \AA}^{-1}$  and an intercept that yields  $2J_0 = (2.4 \pm 0.4) \times 10^4 \text{ mT}$ . Our data for the distance dependence of  $2J$  implies that  $\beta = 0.5 \pm 0.1 \text{ \AA}^{-1}$ , which is consistent with our previous estimates of  $\beta$  for charge recombination in related systems.<sup>48</sup>

(43) Marcus, R. A. *J. Chem. Phys.* **1956**, *24*, 966.

(44) Closs, G. L.; Miller, J. R. *Science (Washington, D.C., 1883-)* **1988**, *240*, 440–447.

(45) Devault, D. *Quantum Mechanical Tunneling in Biological Systems*; Cambridge University Press: Cambridge, 1984.

(46) Newton, M. D.; Sutin, N. *Annu. Rev. Phys. Chem.* **1984**, *35*, 437–480.

(47) Marcus, R. A.; Sutin, N. *Biochim. Biophys. Acta* **1985**, *811*, 265–322.

(48) Lukas, A. S.; Bushard, P. J.; Wasielewski, M. R. *J. Phys. Chem. A* **2002**, *106*, 2074–2082.

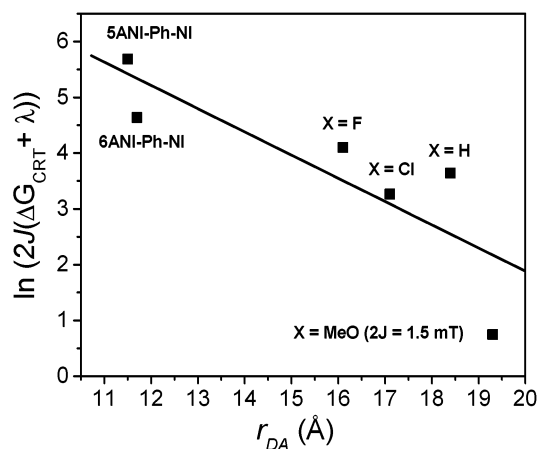


**Figure 8.** Plot of  $\ln(2J(\Delta G_{\text{CRT}} + \lambda))$  vs distance for the indicated dyads and triads.

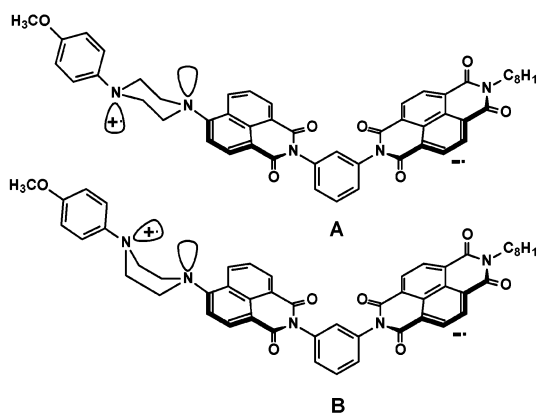


**Figure 9.** Two conformations of  $\text{MeOAn}^+ - 6\text{ANI} - \text{Ph} - \text{NI}^-$  resulting from chair–boat inversion of the piperazine ring.

One of the most striking features of the MFE data for  $\text{MeOAn}^+ - 6\text{ANI} - \text{Ph} - \text{NI}^-$  is the two resonances observed at 1.5 and 15 mT, Figure 7B. The observation of two distinct values for  $2J$  suggests two distinct values for  $r_{DA}$ . The energy-minimized structure of  $\text{MeOAn}^+ - 6\text{ANI}$  is assumed to correspond to the smaller of the two values of  $2J$ , which is used as a data point in the plot of  $\ln(2J(\Delta G_{\text{CRT}} + \lambda))$  vs  $r_{DA}$  in Figure 8. The distance that corresponds to the observed resonance at 15 mT can be obtained using this value,  $\alpha = 0.5 \text{ \AA}^{-1}$  and  $2J_0 = 2.4 \times 10^4 \text{ mT}$  obtained from the fit to the data in Figure 8,  $r_0 = 3.4 \text{ \AA}$ , and eq 6 to yield  $r_{DA} = 18.2 \text{ \AA}$ . This distance is 1.1  $\text{\AA}$  shorter than the 19.3  $\text{\AA}$  distance obtained for  $\text{MeOAn}^+ - 6\text{ANI} - \text{Ph} - \text{NI}^-$  from the energy-minimized structures of the radical cation and anion. This small change in distance is best explained by assuming that there is a secondary minimum energy structure.

The most likely source of two conformations within the radical ion pair is a chair  $\leftrightarrow$  boat interconversion of the piperazine ring, Figure 9. The radical ion pair distance is reduced slightly in the boat conformation (B), resulting in additional Coulombic stabilization of the radical ion pair. While this small degree of “harpooning” due to Coulombic attraction of the two charges may occur,<sup>49</sup> our MFE data do not support larger structural changes due to this mechanism. For example, folding the  $\text{MeOAn}^+$  radical cation over 6ANI decreases  $r_{DA}$  to values

(49) Lauteslager, X. Y.; van Stokkum, I. H. M.; van Ramesdonk, H. J.; Brouwer, A. M.; Verhoeven, J. W. *J. Phys. Chem. A* **1999**, *103*, 653–659.

less than or equal to those within the dyads and would give rise to a second resonance within the triads at much higher fields, which is not observed. Earlier work suggests that deviations from a zigzag arrangement of saturated bonds diminishes the through-bond coupling for electron transfer reactions.<sup>50,51</sup> However, the transannular interaction of the nitrogen lone pair orbitals depicted in Figure 9, structure B, most likely results in slightly enhanced electronic coupling consistent with the modest 15 mT value of  $2J$ .

The possibility of two conformations, however, does not ensure the observation of two distinct  $2J$  resonances. To observe distinct resonances, the time constant for interconversion must be slow relative to the energy difference between the resonances. The difference in  $2J$  values within  $\text{MeOAn}^+ - 6\text{ANI} - \text{Ph} - \text{NI}^-$  is 13.5 mT, which corresponds to a transform-limited time of approximately 0.4 ns. Thus, interconversion of the A and B conformers, if it does occur, must occur at times slower than 0.4 ns to observe distinct resonances. The energy barrier for ring inversion in  $N,N'$ -dimethylpiperazine measured by NMR is 13 kcal/mol.<sup>52,53</sup> Assuming Arrhenius behavior and a prefactor of about  $10^{13} \text{ s}^{-1}$ , this corresponds to an inversion rate of only about  $4 \times 10^3 \text{ s}^{-1}$ . However, in a radical ion pair the Coulombic attraction of the charges (harpooning) can increase the chair  $\rightarrow$  boat inversion rate substantially. For example, Lauteslager et al.<sup>54</sup> have observed that harpooning occurs with rate constants of about  $10^8 - 10^9 \text{ s}^{-1}$  in photogenerated radical ion pair compounds having an  $N$ -phenylpiperidine donor attached to a cyanonaphthalene acceptor. These rate constants are consistent with our data for  $\text{MeOAn}^+ - 6\text{ANI} - \text{Ph} - \text{NI}^-$ . From the amplitude of the two resonances, there appears to be a preference for the A conformation with the longer 19.3 Å distance. However, it must be remembered that for such small  $2J$  values HFIs play a significant role in driving RP-ISC. While both resonances within  $\text{MeOAn}^+ - 6\text{ANI} - \text{Ph} - \text{NI}^-$  have contributions from hyperfine and exchange interactions, the relative magnitude of HFI is significantly greater at the lower field resonance. Therefore, the amplitudes of the two resonances do not necessarily reflect the relative populations of the two radical ion pair conformations.

- (50) Oliver, A. M.; Craig, D. C.; Paddon-Row, M. N.; Kroon, J.; Verhoeven, J. W. *Chem. Phys. Lett.* **1988**, *150*, 366–373.  
(51) Wasielewski, M. R.; Niemczyk, M. P.; Johnson, D. G.; Svec, W. A.; Minsek, D. W. *Tetrahedron* **1989**, *45*, 4785–4806.  
(52) Harris, R. K.; Spragg, R. A. *Chem. Commun.* **1966**, 314–316.  
(53) Abraham, R. J.; Macdonald, D. B. *Chem. Commun.* **1966**, 188–189.  
(54) Lauteslager, X. Y.; Bartels, M. J.; Piet, J. J.; Warman, J. M.; Verhoeven, J. W.; Brouwer, A. M. *Eur. J. Org. Chem.* **1998**, 2467–2481.

The  $\text{XAn} - 6\text{ANI} - \text{Ph} - \text{NI}$  triads, where  $X = \text{H}, \text{F},$  and  $\text{Cl}$ , are structurally similar to  $\text{MeOAn} - 6\text{ANI} - \text{Ph} - \text{NI}$ , differing only in the substituent on  $\text{XAn}$ . However, they have substantially larger values for both  $2J$  and  $B_{1/2}$ . The spin density calculations show that the spin is more strongly localized on the nitrogen atom of  $\text{XAn}$  (N3) within these triads, which results in a decrease in  $r_{\text{DA}}$ . Due to their structural similarity, it is likely that the radical pairs within all of the triads have both A and B conformers. However, the greater line widths within the triads where  $X = \text{H}, \text{F},$  and  $\text{Cl}$  prohibit resolving the two resonance peaks.

## Conclusions

We have shown that the effect of applied magnetic fields on the RP-ISC yield of triplet products within a series of structurally rigid compounds with fixed distances allows for evaluation of the spin–spin exchange interaction,  $2J$ , as a function of  $r_{\text{DA}}$ , the donor–acceptor distance. For those compounds that exhibit exchange interactions on the order of several tenths of a tesla, the singlet–triplet mixing within the radical ion pair is dominated by the exchange interaction, and  $2J \gg E_{\text{HFI}}$ . However, at larger  $r_{\text{DA}}$  (smaller  $2J$ ),  $E_{\text{HFI}}$  can contribute to the observed resonance significantly, and experimentally observed  $B_{1/2}$  within the triad with the smallest value of  $2J$  agrees very well with the calculated  $B_{1/2}$  value. Changes in both the magnitude and number of  $2J$  resonances can be directly correlated with radical ion pair structure. The relationship between  $2J$  and the electronic coupling matrix element for electron transfer,  $V_{\text{DA}}$ , makes it possible to probe the dependence of  $V_{\text{DA}}$  on subtle changes in molecular structure at an unprecedented level of detail, thereby providing insights into how to optimize structures for efficient electron transfer. This type of detailed understanding of how spin–spin exchange interactions map molecular structure and thereby dictate charge separation lifetimes should prove very useful in the design of systems for photochemical conversion and storage of solar energy.

**Acknowledgment.** This work was supported by the Division of Chemical Sciences, Office of Basic Energy Sciences, U.S. Department of Energy (Grant No. DE-FG02-99ER14999).

**Supporting Information Available:** Details regarding the synthesis and characterization of the molecules used in this study. This material is available free of charge via the Internet at <http://pubs.acs.org>.

JA029062A